A mechanism of membrane topology remodeling and variation in cell morphology

Kakihara, Ken

(Degree)
博士（理学）

(Date of Degree)
2009-03-25

(Date of Publication)
2014-08-12

(Resource Type)
doctoral thesis

(Report Number)
甲4525

(URL)
https://hdl.handle.net/20.500.14094/D1004525

Doctoral Dissertation

A mechanism of membrane topology remodeling and variation in cell morphology

January 2009

Graduate School of Science and Technology
Kobe University

Ken Kakihara

Doctoral Dissertation

A mechanism of membrane topology remodeling and variation in cell morphology

(膜トポロジー変換と細胞形態の多様性を生み出す機構について)

January 2009

Graduate School of Science and Technology
Kobe University

Ken Kakihara

Abstract

The remodeling of plasma membrane topology is a fundamental process in every living organism. The most well known example of membrane topological change is the terminal phase of cytokinesis, when one cell divides and gives rise to two daughter cells. During this process, single plasma membrane, which is a closed surface, undergoes remodeling of topology and finally converts into two plasma membranes, each of them forming individual closed surface.

The plasma membrane topology remodeling also plays an important role during development of epithelial tubular organs, such as the vascular system in vertebrates and the tracheal system in insects. Tubulognesis of these organs involves connection of tubes at their termini, as observed in the anastomosis formation between the capillary veins and arteries. Since each tube are closed at the terminus before the connection, cells at the tip of tubular branch remodel plasma membrane topology. After the initial contact between the tip cells, each of them converts into torus topology, a doughnut-like shape, thus the tubes are connected through the hollow in the cell body (Kamei et al., 2006, Samakovlis et al., 1996b).

Prior to the cell topology change in the epithelial tube connection, vesicles assemble at the future hollow. This assembly is reported in both the vertebrate and the insect system, and it is hypothesized that this event is playing an essential role for

doughnut-like shape formation (Kamei et al., 2006, Lee and Kolodziej, 2002). Up to now, almost nothing is known about the molecular machinery behind this plasma membrane topology remodeling.

In order to understand the mechanism of cell topology remodeling during tube connection, I used the *Drosophila* embryonic tracheal system as a model. I assumed that cells at the tip of tracheal tubes called the fusion cells, which undergo cell topological change, specifically express a set of genes for topology conversion. Utilizing the public database at Berkeley (Tomancak et al., 2002), I identified ADP-ribosylation factor-like 3 (Arl3 or CG6560) as a candidate gene.

Arl3 is an evolutionarily conserved small GTPase, and belongs to the ADP-ribosylation factor family, which is known to regulate vesicle traffic (D'Souza-Schorey and Chavrier, 2006). In *Drosophila* embryos, Arl3 protein was specifically expressed in the tracheal fusion cells. Spatio-temporal analysis of Arl3 protein distribution suggested that Arl3 expression starts just before the hollow formation, and Arl3 localized at the vesicles at the future hollow area.

In the Arl3 mutants, fusion cells were apparently normal in terms of their cell adhesion activity and vesicle assembly at the future hollow. But the topology remodeling did not occur, and the tube was not connected. Time lapse analysis of tracheal cell morphology showed that in Arl3 mutants, plasma membrane within fusion cells become near to each other to a distance impossible to distinguish by confocal

microscopy, but the tube was not connected. These results indicate that Arl3 is playing an important role, specifically during fusion of two separate plasma membranes in each fusion cell.

Arf family proteins shown to directly bind to lipid bi-layer, thereby inducing local positive membrane curvature. This induction is thought to be required for membrane fission or fusion events (Lundmark et al., 2008). I propose that, Arf family proteins are not only used for generating intracellular membrane curvature, but it is used in the context of topology remodeling of entire plasma membrane itself.

1. Introduction

Stable maintenance of cell surface topology is an essential property of plasma membranes in keeping individuality and shape of the cell. In special situations during development, plasma membranes change their topology through membrane fusion. Cellularization of insect blastderm proceeds by ingression of the plasma membrane of syncytium around each nucleus and its fusion to individualize cells (Foe et al., 1993). On the other hand, fusion of myoblasts via the outer layer of plasma membranes forms multinucleated myotubes, and its molecular mechanism has just begun to be revealed (Kim et al., 2007; Massarwa et al., 2007). Fusion of plasma membrane via inner layer of membrane takes place in every round of cell cycle in the process called abscission at the finishing stage of cytokinesis (Gromley et al., 2005). During development of tubular organs, such as inter-segmental vessel formation in the zebrafish (Kamei et al., 2006), alignment of intracellular vesicles in a row and their fusion with plasma membranes converts spherical cells into hollow unicellular tubule. Despite its importance in vasculogenesis and cell topology studies, research progress toward understanding of intracellular plasma membrane fusion has been slow.

Fusion of the *Drosophila* tracheal tubules offers a unique opportunity to study internal plasma membrane fusion in genetically tractable model system (Samakovlis et al., 1996b; Tanaka-Matakatsu et al., 1996). The *Drosophila* tracheal system is derived from invagination of the tracheal primordium in ten metameres of each side of embryos

(Samakovlis et al., 1996a). Each primordium extends tubular branches in stereotypical patterns. Branches for dorsal trunk (DT) and lateral trank (LT) meet at specific locations at segment boundaries and dorsal branch (DB) and ventral branch (VB) meet at dorsal and ventral midline, respectively. Fusion is initiated by contact of specialized fusion cells that are located at the tip of each branch. Detailed studies on fusion of DT have revealed that fusion cells in contact establishes new adherens junction between them. Inside of fusion cells, tracks of microtubules associated with F-actin and vesicles align along the long axis of branches in a pattern prefiguring the future luminal axis ((Lee and Kolodziej, 2002), Fig. 1A, time 15'00", Fig. 1D). Although less is known, similar intracellular event is believed to mediate fusion of other branches. In each case, change of fusion cell shape from sphere to torus, a doughnut shape, is the key event for connection of two closed branches into one continuous tube. But the molecular machinery of cell topology conversion remained completely unknown.

One proposed mechanism for cell shape conversion of tracheal fusion cells is that microtubule tracks guide vesicle assembly and facilitate internal fusion of plasma membranes bridged by the tracks (Lee and Kolodziej, 2002). This model predicts that those vesicles fuse with plasma membrane by exocytosis. The exocyst complex is machinery for polarized membrane fusion and exocytosis in various systems, such as the nervous system and epithelial tissues (Hsu et al., 2004; Langevin et al., 2005; Lipschutz and Mostov, 2002; Murthy et al., 2003). Exocyst complex also localizes at

the midbody, the site of abscission during cytokinesis (Gromley et al., 2005), and is required for abscission, suggesting that it is a good candidate for the regulator of internal plasma membrane fusion. Here I report that Arf-like 3 (Arl3) is a candidate molecule for local recruitment of exocyst complex during internal plasma membrane fusion in the tracheal fusion cells.

2. Results

2.1 Identification of Arf-like 3 as a fusion cell vesicle component

To understand membrane dynamics in fusion cells, I first observed the intracellular membrane dynamics by time-lapse imaging of DT fusion cells labeled with the membrane targeted GFP (GFP-CAAX, (Ikeya and Hayashi, 1999)). After the initial contact between fusion cells (Fig. 1A time 0'00", contact site is shown by arrowhead), intracellular array of vesicles (Fig. 1A, time 15'00", arrows) appeared between the contact site of fusion cells and the tip of lumens (Fig. 1A, time 15'00", Fig. 1D, arrows). Finally, lumen penetrated through fusion cells where GFP-CAAX accumulated (Fig. 1A, time 69'00", arrowhead). These observations lead us to investigate the role of intracellular vesicles during tracheal tube connection.

In order to identify genes involved in tracheal branch fusion, I searched BDGP *in situ* database (Tomancak et al., 2002) for genes expressed in a subset of *Drosophila* tracheal cells and identified Arf-like 3 (Arl3, CG6560 (Drysdale and Crosby, 2005)). Antibody against Arl3 detected specific expression in all tracheal fusion cells (Fig. 1B, data not shown), and this pattern was consistent with the RNA expression pattern ((Tomancak et al., 2002); data not shown). Accumulation of Arl3 become prominent when the pair of fusion cells approached within ~10 μm from each other, and persisted after completion of fusion (Fig. 1B, data not shown). High magnification view revealed that Arl3 was detected in vesicular pattern within fusion cells, and co-localized

with the intracellular vesicles marked by GFP-CAAX (Fig. 1D). In addition Arl3 was detected in sensory organs from embryonic stage 15 (data not shown).

2.2 Arl3 is an N-terminally acetylated microtubule associated protein

Arl3 is a member of ADP-ribosylation factor (Arf) sub-family of Ras-like small GTPases, and its structure is evolutionary conserved from yeast to human ((Kahn et al., 2005), Fig. 2A). Arf family members play various roles in intracellular vesicle traffic (Burd et al., 2004; Kahn et al., 2005; Kawasaki et al., 2005; Nie et al., 2003). Arf-like family members, such as human Arl8 and *S.* cerevisiae Arl3p (also known as Arfrp, Arf-related protein, in higher eukaryotes), have been reported to be post-translationally modified at their N-termini (Behnia et al., 2004; Hofmann and Munro, 2006; Setty et al., 2004). To detect post-translational modification, Arl3 expressed in *Drosophila* S2 cells was immunopurified and subjected to mass spectrometric analysis. A number of peptide fragments corresponding to the mass of acetyl group linked to the second glysin (G2) residue of the N-terminus of Arl3 were detected (Fig. 2B, arrows). In addition, unmodified peptides missing the N-terminal methionine were also detected (precursor ion: 771.98 m/z (1+), data not shown). The result suggests that *Drosophila* Arl3 undergoes removal of methionine and subsequent acetylation at the N-terminus. No peptide peaks corresponding to N terminal myristoylation were detected. N-terminal acetylation was reported to be crucial for yeast

Arl3p to localize at golgi apparatus and N-terminal aceylation and N-terminal hydrophobic residues are required for human Arl8 to localize at lysosomes (Behnia et al., 2004; Hofmann and Munro, 2006; Setty et al., 2004). To address the functional significance of N-terminal acetylation, GFP was fused to the N-terminus of Arl3. GFP-Arl3 migrated in SDS-PAGE with the molecular mass expected for full-length fusion, suggesting that the cleavage at G2 was prevented by the GFP fusion (Fig. 2C, data not shown). Unlike endogenous Arl3, GFP-Arl3 expressed in tracheal cells was distributed uniformly (Fig. 2D, compare Fig. 1D), suggesting that the N-terminal GFP fusion prevented vesicle association of Arl3. The results suggest that N-terminal acetylation is required for association of Arl3 with intracellular vesicles.

Mammalian Arl3 has been reported to associate with microtubules (Grayson et al., 2002), and the *S. pombe* counterpart of Arl2/3, Alp41, has been reported to be involved in regulation of microtubules (Radcliffe et al., 2000). I therefore performed a biochemical test to ask if Arl3 associates with microtubules. S2 cells expressing Arl3 were lysed in hypotonic buffer and the cell lysates were centrifuged at 100,000 g and analyzed by Western blotting (Fig. 2C). α-tubulin was efficiently pelleted by this procedure. Addition of the microtubule destabilizing drug nocodazole (NZ) translocated α-tubulin from the pellet to supernatant fraction, suggesting that the pellet fraction contained polymerized microtubules. Arl3 was also efficiently pelleted without NZ, and addition of NZ translocated Arl3 from pellet to supernatant. C-terminal GFP fused Arl3

(Arl3-GFP) was almost completely soluble in the absence of nocodazole. N-terminal GFP fusion (GFP-Arl3) caused partial solubilization. These results indicate that Arl3 associate with microtubules either directly or indirectly, in a manner requiring its intact C-terminus.

2.3 Arl3 is required for fusion of tracheal branches

Arl3 is located in the section 93F of chromosome 3. Its 5' exon overlapped with CG6678 that was transcribed from the opposite strand. One P-element insertion P{XP}d10234 was found in this region. Since homozygous P{XP}d10234 embryos expressed a detectable amount of Arl3 in tracheal fusion cells and underwent apparently normal fusion in the DT (data not shown), I attempted to isolate deletions of the *Arl3* locus by imprecise excision of P{XP}d10234. One of such deletion $Arl3^{1}$ removed 680 bps including the first exon of *Arl3* containing the starter methionine codon (Fig. 3A, chromosome 3R:17712548-17713227, coordinate based on *Drosophila* melanogaster genome assembly r5.3, (Crosby et al., 2007)). $Arl3^{1}$ additionally disrupted 5' UTR of *CG6678*. Since Arl3 protein was undetectable in homozygous $Arl3^{1}$ embryos (Fig. 1C, compare with Fig. 1B), I considered $Arl3^{1}$ as a molecularly defined null allele of *Arl3*. While control embryos were completely successful in fusion of the DT (360 successful fusion in 360 fusion point scored in 20 embryos, Fig. 3B, C), homozygous or hemizygous $Arl3^{1}$ embryos showed high frequency of disconnection phenotype in DT

(*Arl3*^{1}/*Arl3*^{1}: 38/162 in 10 embryos; *Arl3*^{1}/*Df(3R)e-GC3*: 22/135 in 10 embryos). Failure of fusion was more severe in DB (data not shown). To exclude a possible contribution of CG6678 in tracheal fusion, I attempted to rescue the mutant phenotype of *Arl3*^{1} by tracheal-specific expression of Arl3. Wild type Arl3 rescued DT fusion to 87.5% (126/144 connected, from 8 embryos, Fig. 3B, Full length). Putative GTP bound form of Arl3 (Q71L) was more effective in the rescue assay (97.9%, 132/135 connected in 8 embryos, Fig. 3B, C, GTP form). The putative GDP bound form Arl3(T31N) also rescued the phenotype to some degree (Fig. 3B, GDP form). From these results, I conclude that Arl3 is essential for fusion of tracheal branches.

2.4 Arl3 is required for internal fusion of plasma membrane

To further understand the function of Arl3 in branch fusion, I focused on fusion of DT, where detailed description of cytoskeleton and cell membrane dynamics is available (Lee and Kolodziej, 2002; Tanaka-Matakatsu et al., 1996) (Fig. 1A). The phenotypes described here were observed in more than 70% of the case in DT and represents the Arl3 mutant phenotype. I first conducted time-lapse analysis of F-actin dynamics during fusion of DT. In control embryos (Fig. 4A), tips of tracheal lumen in stalk cells decorated with dense F-actin (Fig. 4A, time 0'00", asterisks) shifted their position to each other, become closely apposed (time 16'30", arrowhead), and connected (time 62'00", arrowhead). In *Arl3*^{1} mutants, tips of tracheal lumen shifted

and apposed tightly to each other in a manner similar to control embryos, but remained unconnected (Fig. 4B, time 110'00", arrowhead). The pair of fusion cells maintained attachment for the next few hours but often detached when vigorous muscular activity started in stage 17 (data not shown).

Tracheal branch fusion is preceded by the formation of microtubule tracks that marks the future luminal axis, where intracellular vesicles accumulate (Lee and Kolodziej, 2002) (Fig. 4C, D, 1D). In Arl3 mutants, microtubule track formation (compare Fig. 4C and 4F, arrows) and vesicle accumulation along the track appeared normal (Fig. 4D and 4G, arrows), and E-cadherin was accumulated normally at the contact interface of apposed fusion cells (Fig. 4E and H, arrowhead). I also used chitin binding probe (CBP) to detect luminal extracellular matrix (ECM; Fig. 4E, magenta). Since chitin is synthesized by secreted chitin synthesizing enzymes and their substrate, CBP staining reveals apical exocytosis activity in tracheal cells. In Arl3 mutants, I often detected dots of CBP-positive region between two apposed fusion cells that have failed to fuse (Fig. 4H, arrowhead, magenta). This "island" of CBP-positive region corresponds to the space between two fusion cells in contact, suggesting that Arl3 mutants are able to form apical membrane and accumulate luminal ECM. The confinement of luminal ECM also suggests that a ring-shaped adherence junction surrounding the Island of CBP was functional (Fig. 4H, arrowhead). In addition, the distribution of apical proteins Crb and aPKC were not affected in Arl3 mutants (data not

shown).

To further investigate the role of Arl3 in targeting apical exocytotic vesicles including luminal ECM in fusion cells, I studied the behavior of GFP fusion of luminally secreted chitin deacetylase Serpentine ((Luschnig et al., 2006)) in dorsal branch where high-resolution imaging is possible. Serpentine is transported to apical surface facing the luminal side of tracheal tube, thus serpentine-GFP ((Luschnig et al., 2006)) enables the time-lapse observation of apically targeted vesicles. Serp-GFP and mCherry-CAAX were co-expressed to monitor luminal ECM and cell morphology (Fig. 5A). In the control embryos, dorsal branch fusion cells that have contacted with each other have no Serp-GFP signal in region between two tips of existing lumen (Fig. 5A, time 0'00", region between two asterisks). In the next 10 minutes, the lumen tips become closer (~ 3μm), a faint line of serp-GFP appeared within the cytoplasm of fusion cells flanked by lumen tips (Fig. 5A, time 8'10", arrow). This GFP signal became stronger and fusion was completed in the next 30 minutes (Fig. 5A, time 37'05", arrowhead). This intracellular accumulation of serp-GFP between lumen tips is likely to represent accumulation of exocytotic vesicles for secretion of apical ECM and reveals future luminal axis formation. In Arl3 mutants, fusion cells made contact with each other (Fig. 5B, time, 0'00"). Faint but distinct Serp-GFP signal between the lumen tips were detected (Fig. 5B, time 5'00", green, arrow). However this signal remained weak and lumen was not connected (Fig. 5B, time 40'45", arrowhead). This analysis

confirmed that Arl3 mutant fusion cells are capable of contacting each other, and apically targeting vesicles containing luminal ECM components to the future lumen axis, but the mutant cells fail to complete fusion.

From these results, I conclude that organization of microtubule tracks, vesicle assembly along them, and E-cadherin-dependent cell adhesion was normal in fusion cells of Arl3 mutants. Assembly of apical cell membranes and secretion of luminal ECM were also unaffected. I thus concluded that Arl3 is specifically required for intracellular fusion of plasma membranes.

2.5 Arl3 is required for targeting exocyst complex to fusion site

I next tested the possible involvement of the exocytosis machinery in internal plasma membrane fusion in fusion cells. Sec5, a key component of the exocyst complex, was ubiquitously expressed and accumulated in vesicles that were often located beneath plasma membrane (Fig. 6A; (Murthy et al., 2003)). Sec5 was enriched at apical membranes of tracheal lumens where massive exocytosis of luminal ECM and apical cell membranes takes place (Fig. 6A). I also noted that Sec5 was enriched at the contact site of fusion cells in a pattern correlating with the microtubule tracks (Fig. 6A, arrowhead). Sec5 signal partially overlapped with Arl3 within fusion cells, where lumen will form (Fig. 6C, arrowhead). In Arl3 mutants, Sec5 accumulation at the contact site was greatly decreased while Sec5 signals associated with apical membrane facing the

lumen remained the same (Fig. 6B, compare magenta signals at arrowhead and asterisk with Fig. 6A).

To understand the dynamics of Sec5 during tracheal tube connection, I performed time-lapse imaging of Sec5-GFP during fusion of DB with high-resolution imaging. Sec5-GFP showed rapid cycle of accumulation and disappearance (half-life shorter than 30") underneath apical membranes (Fig. 6D). When the tip of lumen in the pair of fusion cells approached within 3 μm, when future luminal axis is formed in DB (Fig. 5), Sec5-GFP was accumulated at the contact site and the signal intensity was increased as the fusion proceeded (Fig. 6F, plot in magenta, N=2). In Arl3 mutants, accumulation of Sec5-GFP did not increase despite the distance between lumen tips became less than 3 microns (Fig. 6E, F, N=3).

Next, I examined the requirement of Sec5 for tracheal tubule connection. In homozygous *sec5* mutants, DT appeared normal but DB fusion points were broken at nearly all positions (Fig. 6G, H). Fusion of dorsal branches was also sensitive to half reduction of the gene dosage of *Arl3* (32/60, 6 embryos) and *sec5* (34/40, 5 embryos; Fig. 6I). Combination of *Arl3*/+ and *sec5* /+ significantly enhanced the phenotype compared to each single mutation (9/40, 4 embryos; Fig. 6I). From these results, I conclude that Arl3-dependent accumulation of Sec5 to the contact sites of fusion cells is essential for internal plasma membrane fusion within fusion cells.

2.6 Interaction of phospholipids and Arf-like 3 *in vitro*

In this work, I have shown that Arf-like 3 is required for tracheal fusion cell topology conversion. Experimental results on the involvement of exocyst complex during tracheal tube fusion suggest that membrane fusion machinery is recruited to the narrow space between the pre-existing apical domain and the newly formed apical domain in an Arf-like 3 dependent manner for membrane fusion. The remaining question to be solved is how this local accumulation of exocyst complex is achieved. Direct binding of Sec5 to Arf-like 3 is unlikely, since I could not detect binding of Sec5 and Arf-like 3 by co-immunoprecipitation experiment in the S2 culture system.

One hypothesis is that membrane fusion machinery favors high curvature membrane zone for localized lipid bi-layer fusion (James, J., et al., 2008, Marten, S., et al., 2008, Begele, Al, et al., 2009). Arf family of small GTPases are shown to induce membrane curvature (Lee, M., et al., 2005, Lundmark, R. et al., 2008). So, Arf family member related Arf-like 3 might have similar function on membrane structure.

To examine the membrane curving activity of Arf-like 3, I purified Arf-like 3 protein from Baculo-virual expression system (Fig. 8A). N-terminal acetylation of recombinant Arf-like 3, the modification thought to be required for membrane association of Arf-like family members, was confirmed by mass spectrometry analysis (Fig. 8B). Preliminary result suggests that Arf-like 3 directly binds to reconstituted liposomes *in vitro* (Fig. 8C). Further more, Arf-like 3 showed specific binding to phosphatidic acid (PA), in a

GTP-loading dependent manner (Fig. 8D).

3. Discussion

3.1 Function of Arl3 in vesicle trafficking and tracheal tube connection

Connection of tracheal tubules involves fusion of inner plasma membranes at restricted areas, which results in formation of the luminal cavity through the cell body of fusion cells. Here I have provided evidences that Arl3 plays key roles in converting cell surface topology of fusion cells. Fusion cells in contact with each other develop microtubule tracks that bridge the two separate apical membranes: one facing the existing luminal space and the other that forms *de novo* at the contact site of fusion cells. I have shown that Arl3 associates with both vesicles and microtubules. The presence of N-terminal acetylation suggests Arl3 associates with vesicle membranes via its N-terminus (Fig. 2B, D). Since C-terminal fusion of GFP blocked microtubule association of Arl3, intact C-terminus seems to be important for association with microtubules (Fig. 2C). Such modular structure of Arl3 suggests that it is capable of bringing vesicles to microtubules. The location of Arl3-positive vesicles near microtubule tracks in fusion cells supports this idea (compare Fig. 1D and 4C).

I have also shown that Sec5 localizes at the microtubule tracks in fusion cells. Time-lapse observation of Sec5-GFP suggests that Sec5 accumulates at the positions where apical membranes are assembled. The specific requirement of Arl3 for Sec5 localization at the position of internal plasma membrane fusion, and genetic requirement for Arl3 and Sec5 for fusion suggest that Arl3 is required for the

recruitment of exocyst complex to the site of fusion. Arl3 and Sec5 partially overlapped in vesicles at the site of fusion (Fig. 6C).

N-terminal acetylated Arl8 enhances the cell peripheral localization of lysosomes in a microtubule dependent manner ((Hofmann and Munro, 2006)). I speculate that Arl3 is acting in a similar fashion as Arl8 to regulate localization of Sec5 positive vesicle compartment along microtubules to the contact site of fusion cells. Fig. 7 shows our current model of Arl3 function. Arl3 regulates Sec5 positive vesicle trafficking on microtubules at the future luminal axis, and directs fusion of closely apposed plasma membranes to convert cell topology.

Although our results suggest that Arl3 regulates Sec5-dependent exocytotic event, its function is limited to a specific subset exocytosis. E-cadherin trafficking to the plasma membrane was reported to involve Sec5 in other epithelial cell types (Langevin et al., 2005), but Arl3 mutation did not affect cell surface presentation of E-cadherin in fusion cells. In addition Arl3 did not play any significant role in other exocytosis-dependent processes such as the deposition of luminal ECM and assembly of apical membranes at the contact site of fusion cells. Such a high selectivity of the Arl3 function might be explained by heterogeneity in exocytosis pathways.

When this work was in the final stage, an independent work on *Drosophila* Arl3 has been published on line (Jiang et al., 2007). The authors used the weak $Arl3^{XP[d10234]}$ allele and reached a conclusion that is in principle in good agreement with

our results and consolidates the notion that Arl3 is a key effector of tracheal tubule fusion.

3.2 Similarity between cell topology conversion in fusion cells and cytokinesis

Abscission separates two daughter cells at the end of cytokinesis. I noted several similarities between abscission and tracheal branch fusion. During abscission, vesicles containing exocyst complex including Sec5 accumulate at narrow channels of plasma membrane at the midbody, and massive fusion of those vesicle with each other and with plasma membrane between them divides the plasma membrane into two daughter cells. Gene knockdown analyses on mammalian cultured cells demonstrated that abscission requires Sec5 (Gromley et al., 2005). Interestingly, Arl3 was also detected in midbody and its knockdown phenotype caused incomplete cytokinesis (Zhou et al., 2006). Such a similarity of abscission to tracheal fusion suggests that they may share a common underlying mechanism of inner membrane fusion involving Arl3 and exocyst complex. One notable difference between them is that during abscission, membrane fusion takes place at the entire surface of plasma membrane encircling the midbody. On the other hand, membrane fusion in tracheal fusion cells takes place between two separate domains of apical membranes. This difference in the shape of plasma membrane utilized for fusion explains the difference in topological consequences in cell shapes: two spheres versus a torus.

3.5 Interaction of lipid bi-layer and Arf-like 3

In this study, I have shown that Arf-like 3 localizes at the intra-cellular vesicles and is required for fusion cell topology conversion that is essential for tracheal tube connection. Arf-like 3 directly binds to lipid bi-layer in the liposome-binding assay, and showed preferential affinity to phosphatidic acid (PA). Based on these observations, I discuss two models of fusion cell topology conversion and possible function of Arf-like 3.

One model is direct fusion of opposing plasma membrane. I assume that direct fusion is unlikely, since Sec5, the key component of Exocyst complex, is targeted to the site of membrane fusion in an Arf-like 3 dependent manner, and Sec5 is required for tube connection. The Exocyst machinery regulates the fusion of intra-cellular vesicles with the plasma membrane, so the requirement of Exocyst machinery suggests involvement of intra-cellular vesicles during tracheal tube connection.

In the second model, two plasma membranes simultaneously fuse with one class of intra-cellular vesicles. The sub-cellular localization of Arf-like 3 is mainly on the cytoplasmic vesicles, which suggests that Arf-like 3 functions on the vesicles. Arf-like 3 might be targeted to the subset of vesicles that are enriched with PA, and might be required for the fusion between vesicle-to-vesicle fusion and / or vesicle to plasma membrane fusion mediated by the Exocyst complex. It is also possible that Arf-like 3 functions on the plasma membrane. Phosphatidic acid (PA) might induce the

local accumulation of Arf-like 3 *in vivo*, as suggested from the case of *in vitro* experiment. If PA preferentially accumulates at the tip of *de novo* and / or pre-existing apical region within fusion cells, Arf-like 3 might be recruited to the site of plasma membrane fusion and enhances the vesicle to plasma membrane fusion. Monitoring the localization of PA within fusion cells, and perturbing the PA level might give some hints to gain more insight into the machinery of membrane topology conversion.

Membrane tabulating activity of Arf-like 3 is currently not detected in the experimental condition designed for F-BAR domain protein (data not shown). This result may be due to the slow nucleotide exchange rate of Arf-like 3 among Arf family proteins (Cavenagh, M., et al., 1994). Assessment of nucleotide loading condition for recombinant Arf-like 3, and the buffer condition for membrane tubulation are required to further examine the function of Arf-like 3 *in vitro*.

3.4 Possible functions of mammalian Arl3

One notable difference of *Drosophila* Arl3 from its mammalian counterparts is its highly restricted expression in postmitotic tracheal fusion cells and sense organs. This makes striking contrast to the expression and requirement for mouse Arl3 in wider range of tissues (Schrick et al., 2006). I speculate that *Drosophila* Arl3 has been co-opted for specialized functions in postmitotic cells and its possible mitotic function may have been taken over by related molecules such as Arl2.

Arl3 mutant mice exhibited a variety of defects including abnormal development of renal, hepatic, and pancreatic epithelial tubule structures (Schrick et al., 2006). Arl3 mutant mice also exhibited photoreceptor degeneration phenotype. It is worth pointing out that outer segment of photoreceptor undergoes the process called disc shedding, in which distal portion of outer segment are constantly detached from the soma and become phagocytosed (Strauss, 2005). This process is likely to involve fusion of internal plasma membrane to pinch off the distal segment. It will be interesting to address the function of mammalian Arl3 in membrane organization during disc shedding process.

4. Materials and methods

4.1 Fly strains

Following fly strains were used in this work. *w; XP[d10234] / TM6B* (Fbal0161143), *w; Df(3R)e-GC3 / TM6B* (Fbab0002775), *y w; FRT42A sec5*^{E10} */ CyO, Kr-Gal4, UAS-GFP* (Fbal0146821, (Murthy et al., 2003)), *y w; esg*^{G66B} */ CyO, hb-lacZ* (Fbal0039323 ((Whiteley et al., 1992)), *y w; btl-Gal4* (Fbtp0001208 (Shiga et al., 1996)), *y w; UAS-GFP-moesin* (Fbtp0017306 (Chihara et al., 2003)), *y w; UAS-GFP-CAAX* (Fbal0119707 (Ikeya and Hayashi, 1999)), *y w; UAS-serp-GFP* (Fbal0196028 (Luschnig et al., 2006)). *Arl3*^{1} was made by imprecise excision of XP[d10234] and was balanced over *TM6B, abdA-lacZ*. The following lines were constructed by the standard transformation method (Sullivan et al., 2000). *y w; UAS-Arl3 (II), y w; UAS-Arl3[Q71L] (II), y w; UAS-Arl3[T31N] (II), y w; UAS-mCherry-CAAX, y w; UAS-GFP-Arl3, y w; UAS-sec5-GFP*.

4.2 Antibodies

For production of anti-Arl3 antiserum, the full length Arl3 protein was fused to GST, purified using gluthatione column (Amersham) and injected into rabbits. The antiserum was used at 1/2500 dilution. Other antibodies are listed below. anti-GFP (mouse, Santa Cruz, 1/500), anti-GFP (rabbit, MBL ,1/500), Dcad2 (rat, DSHB, 1/20), anti-Crb (DSHB), anti-aPKC (Santa Cruz, 1/500), anti-alpha-tubulin (mouse, Sigma DM1A, 1/2),

anti-lacZ (rabbit, Cappel, 1/1000), anti-Sec5 (mouse, 1/10 and TSA; (Murthy et al., 2003)), CBP-Rhodamine (NEB, 1/200). Embryos were fixed and stained as described (Chihara et al., 2003).

4.3 Microscopy

Fixed embryos were imaged with Olympus FV500 confocal scanning microscope equipped with 60x water immersion lens (NA=1.2), and Ar (488nm) and He/Ne (543nm, 633nm) lasers. Time-lapse images were taken with Olympus FV1000 confocal scanning microscope equipped with 60x oil immersion lens (NA = 1.42), and LD473 nm and LD559 nm lasers. Images were enlarged up to 10x with digital zoom. Time-lapse interval and thickness and number of z-slices are: 30", 1μm x 10 slices (GFP-CAAX and GFP-moesin imaging of DT); 30", 0.5μm x 6 slices (sec5-GFP in DB); 5", single slice for serp-GFP and mCherry-CAAX. Time-lapse images were filtered with 2μm radius median filter and 2μm radius Gaussian filter. House developed codes written in Objective-C and Ruby were used in combination with Image J for image processing, movie encoding and intensity analysis.

4.4 Biochemistry

Microtubule association assay: S2 cells were co-transfected with UAS expression vectors and pWAGal4 using Effectene (QIAGEN). 48 hours after transfection, medium

was changed to fresh medium with or without 5μM of nocodazole and cells were incubated at 4℃ for 15 minutes. Samples were kept at 4℃ to avoid repolymerization of tubulin monomers. Cells were resuspended in 25mM Hepes pH 7.0 with protease inhibitor (Complete mini EDTA-free, Roche) with or without 5μM nocodazole and were disrupted by tight Dounce homogenizer. Cell lysate was incubated on ice for 15 minutes and cell debris were removed by centrifugation at 10,000 g for 3 minutes. The supernatant was centrifuges at 100,000 g for 1 hour 4℃. Equivalent amounts of sample were analyzed by Western blotting.

4.5 Mass spectrometry analysis

S2 cells were transfected with pWAGal4 and pUAST-Arl3 plasmids. 48 hours after transfection, cells were harvested and cell lysate was prepared in lysis buffer (25mM Tris-HCl pH 7.0, 150mM NaCl, 0.1% TritonX-100, Complete mini EDTA-free) by sonication. Arl3 protein was immunopurified by anti-Arl3 antibody and protein A agarose (Amersham), fractionated by SDS-PAGE and visualized by silver staining (Dodeca Silver staining kit, BIORAD). Band of approximately 20kDa was cut out from the gel and digested by trypsin. Cleaved peptide was extracted by acetonitrile / TFA and subjected to LC-MS/MS. Data analysis was performed by MASCOT.

4.6 Molecular biology

PCR amplification was done by KOD plus (Toyobo) using plasmid DNA as a template. All the clones were sequence checked before experiment. Sec5 was PCR amplified and cloned into KpnI, XbaI site of pUAST-EGFP-C using the following primer set:

Forward: GGGGGTACCCAACATGGCGCCGCAGCCAGTGGTTACGG

Reverse: GGGTCTAGAGGGGTCCTTGACACTGAAGCAGAG

Arl3 was PCR amplified and cloned into EcoRI, BglII site of pUAST or pUAST-EGFP-C using following primer set:

Forward: GGAATTCCAACATGGGTCTGCTATCGCTGTTG

Reverse: GGAAGATCTGGCTTCTTCATATTCTTGCAGACCCAGTCCAT

Coding sequence of mCherry was PCR amplified and cloned into EcoRI, BglII site of pUAST with following primer set. Reverse primer contains coding sequence for CAAX membrane targeting motif of *Drosophila* Ras2.

Forward: GGGGAATTCCAACATGGTGAGCAAGGGCGAGGA

Reverse:

GGGAGATCTCTACATCAGGCAGCACTTCCTCTTGCCCTTCTTGTACAGCTCG

TCCATGCC

Arl3 variant Q71L form was generated inverse PCR from Arl3 coding cDNA by following primer set:

Forward: TGGAAGATACGTCCATATTGGAAGAACTAT

Reverse: CAGACCACCAATATCCCATACATTCAGTTT

Arl3 variant T31N form was generated inverse PCR from Arl3 coding cDNA by following primer set:

Forward: ACGATACTGAAGCAGCTGGCATCGGAGGAC

Reverse: ATTCTTGCCAGCATTATCCAATCCTAGGAG

4.7 Phylogenetic analysis:

Multiple alignment and phylogenetic analysis were done using on-line version of MAFFT ((Katoh et al., 2005)). Phylogenetic tree was drawn using TreeView software ((Page, 1996)). Accession numbers: Human Arl3 (NP_004302.1), Mouse Arl3 (NP_062692.1), Fly Arl3 (NP_650995.1), C. elegans Arl3 (NP_497037.1), Fly Arl2 (NP_476886.1), Human Arl2 (NP_001658.1), Mouse Arl2 (NP_062696.2), C. elegans Arl2 (NP_495779.1), Arabidpsis Arl2 (NP_179430.1), Dictiosterium Arl2 (XP_640825), S. cerevisiae, CIN4 (NP_013858.1), S. pombe Alp41 (AA83522).

4.8 Computer graphics

Blender version 2.42a (Blender Foundation) was used to generate 3D graphics for model figures in Fig. 7.

Acknowledgements

I thank Itoh T. for lipid bi-layer assays, the members of Hayashi lab for valuable discussion, Tom Schwarz, for reagents and fly strains, Stephen Luschnig for fly strain, Roger Tsien for mCherry cDNA. Wada, A., Izumi, Y., Nakamura, A., Tanaka, T., Sato, K., Takizawa, K., Nakayama, J. for advices and regents, DSHB for antibodies, Bloomington stock center and Exelixis for fly strains. I am grateful to Tatsuhiko Noguchi and Tetsu Otani for comments on the manuscript.

Figure legends

Figure 1. Vesicle assembly during tracheal tube connection and expression of Arl3. All figures are presented as anterior left, dorsal up, unless other wise noted. (A) Snapshots of dorsal trunks undergoing fusion, taken from a time-lapse movie of the membrane marker GFP-CAAX. 0'00 ": Two fusion cells have contacted (arrowhead). Asterisks mark the tip of lumen in each branch. Fusion cells are located between the arrowhead and each asterisk. 15'00'': GFP-CAAX-positive signal have appeared as lines connecting the tip of lumen and the contact site (arrows), marking the site of vesicle assembly (clear vesicular staining of fixed preparation is presented in Fig. 1D). 69'00": Fusion completed. Large diameter of lumen is now spanning the entire length of fusion cells.

(B) Late stage 14 embryos was labeled with *btl>GFP-moesin* (Green) and anti-Arl3 (Magenta). Arl3 is detected in fusion cells of DT (arrowhead). Scale bar 30 μm.

(C) Arl3 is not detectable in an $Arl3^{1}$ mutant embryo.

(D) Arl3 is localized in intracellular vesicles. High magnification view of a fusion point of DT labeled with (GFP-CAAX, green) and Arl3 (magenta). Fusion cells are highlighted with dotted line. Contact site between fusion cells are indicated by arrowhead. Arrows indicated overlap of the signals along the future luminal axis. Lumen tips are indicated by asterisk. Scale bar 10 μm.

Figure 2 Phylogenetic and biochemical analyses of Arl3.

(A) Phylogenetic relationship of Arl3 and Arl2 deduced by Nearest Neighbor Joining method. Arl3 and Arl2 comprise two distinct groups. Related yeast proteins Alp41 (S. pombe) and CIN4 (S. cerevisiae) occupy intermediate positions. Scale bar indicates nucleotide substitution per site.

(B) Arl3 is acetylated at second glycine. Spectral profile of LC MS/MS analysis of Arl3 purified from S2 cells. Acetylated N-terminal fragments were detected (b peaks).

(C) Arl3 associated with microtubule. Western blotting analysis of cell extracts treated with or without nocodazole (NZ) after high-speed centrifugation. Lys, total lysate; PPt, pellet fraction; Sup, supernatant. Equivalent amounts of each fraction were loaded.

(D) GFP-Arl3 showed diffuse cytoplasmic distribution.

Figure 3. Characterization of Arl3 mutants.

(A) Genomic structure of the *Arl3* locus. Brackets in the lower line indicate the region deleted in Arl3[1]. Box-and-whisper indicates the structure of the mRNA transcript and solid arrows above indicate the protein-coding region.

(B) Quantification of tracheal phenotypes of Arl3 mutants and rescue by transgenes. The frequency of successful fusion in DT was counted in embryos stained with CBP (solid bar) Error bar indicate standard deviation of phenotypic variability between embryos. Df, Df(3R)e-GC3; GDP form, Arl3-T31N expressed in Arl3 mutant; GTP

form, Arl3-Q71L expressed in Arl3 mutant ; full length, wild-type Arl3 expressed in Arl3 mutant. Transgenes were expressed by btl-Gal4 driver.

(C) Morphologies of DT fusion points of control, $Arl3^{1}$, and its rescue by Arl3-Q71L. Tracheal system was labeled with GFP-moesin. Arrowheads indicate fusion points of tracheal tubes. Scale bar 10μm.

Figure 4 Arl3 mutants exhibited specific defects in internal plasma membrane fusion.

(A) Time course of dorsal trunk fusion in control embryos labeled with F-actin marker GFP-moesin. Lumen tips are indicated by asterisk. Fusion point is indicated by arrowhead.

(B) Phenotype of $Arl3^{1}$. Lumen tips became close to each other but remained discontinuous.

(C-E) control embryos. (F-H) $Arl3^{1}$ embryos. (C, F) Parallel array of microtubules (arrow) runs between lumen tips (asterisk) during tracheal tube connection. Contact site of fusion cells are indicated by arrowhead. This microtubule track formation was not affected in Arl3 mutants. (D, G) Intracelluar vesicles (labeled by GFP-CAAX, green, arrows) align in rows between lumen tips (asterisks) and the contact site (arrowhead) where E-cadherin accumulated (magenta). These expression patterns were unchanged in Arl3 mutants.

(E, H) Fusion points of DT in stage 15 embryos labeled with E-cadherin (green) and the

apical ECM marker CBP (magenta). In a control fusion point, a ring of E-cadherin (arrowhead) encircles the lumen that has become continuous. In Arl3 mutants, the lumen remained discontinuous and developed a small island of CBP-positive space at the contact site.

Figure 5. Time-lapse imaging of apical exocytotic vesicle during lumen connection in dorsal branch.

Cells were labeled with luminal ECM marker Serp-GFP and cell shape marker mCherry-CAAX

(A) Control embryo. 0'00": Fusion cells are in contact and lumen tips are approaching to each other (arrowhead: fusion cell contact site, asterisks: lumen tips). 8'10": Serp-GFP accumulated in a row between lumen tips (arrow). 37'05": Lumen connection is complete.

(B) Arl3 mutant embryo. 0'00": Lumen tips are approaching and fusion cells are in contact. 5'00": Serp-GFP accumulation was detectable between lumen tips. (arrow). 40'45": Lumen was not connected (arrowhead).

Figure 6. Accumulation of Sec5 at the future luminal axis depends on Arl3.

(A-C) fusion points of DT. (A) In control embryos, Sec5 containing vesicles (magenta) accumulated in rows that mark the future luminal axis (region between two asterisks).

Sec5 was enriched at the contact site (arrowhead).

(B) In Arl3 mutants, vesicles containing GFP-CAAX accumulated in rows in future luminal axis (between asterisks and arrowhead) as in control embryos, but Sec5 signal was decreased.

(C) Sec5 partially colocalizaed with Arl3 in control embryos (arrowhead). Lumen tips are indicated by asterisks.

(D, E) Distribution of Sec5-GFP in fusion cells of dorsal branch undergoing fusion. Rectangles indicate the position between the tips of lumens, where accumulation of Sec5-GFP was observed in control (D). In Arl3 mutants accumulation of Sec5-GFP was weak (E). Scale bar: 10 μm.

(F) Quantification of Sec5-GFP signals. Signal intensities in rectangles were plotted over time. Arrows and arrowheads indicate the time when the distance between the tips of lumen reached 4μm and 3μm, respectively.

(G, H) lateral (G) and dorsal (H) views of $sec5^{E10}$ embryos at stage 16 stained with CBP. DT was fused normally, but DB1-5 failed to fuse.

(I) Genetic interaction of Sec5 and Arl3. Frequency of successful fusion in dorsal branch was scored. Compound heterozygotes of $sec5^{E10}$ and $Arl3^{1}$ exhibited significant enhancement of the phenotype compared to each single heterozygotes (Student's t-test, unpaired, two tailed, *: $p = 0.0003$, **: $p = 0.0002$).

Figure. 7 Model of inner plasma membrane fusion during tracheal tube connection

Two fusion cells in contact are shown in green. Microtubules at the future luminal axis are shown in yellow. Intracellular vesicles at the future luminal axis are shown in magenta. Cadherin is shown in red and lumen in white.

(A) Accumulation of vesicles at the future luminal axis. Intracellular vesicles involved in exocytosis align along the microtubule track at the future luminal axis. These vesicles contain Arl3 and Sec5, and are targeted to the contact site of fusion cells.

(B) Inner plasma membrane fusion. Vesicles along the microtubule tracks fuse with plasma membranes and help the expansion of apical membrane. Apical membrane facing the lumen tips protrudes inwardly, and juxtapose to fusion cell contact site. Vesicle-to-vesicle and vesicle-to-plasma membrane fusions occur in this narrow space, and facilitate fusion of plasma membranes, resulting in opening of tubule ends. In loss of Arl3 function, lumen connection halts in the absence of inner plasma membrane fusion.

Figure 8. Lipid bi-layer association of purified Arf-like 3

(A) CBB staining of purified Arl3-3xFlag fusion protein. The band detected approximately 21kDa corresponds to Arl-3xFlag. (B) LC-MS/MS N-terminal fragment of Arl3 is shown. Peptide ion peaks that match the estimated molecular weight is detected. (C) Liposome binding assay result of purified Arl3 protein is shown. Arl3

pre-loaded with GTP, GDP or without nucleotide was incubated either in the presence of liposomes or not. Reaction mixture was subjected to ultra-centrifugation for liposome sedimentation. "s" and "p" stands for supernatant and pellet fraction respectively. Each fraction was detected with western blotting by anti-Flag antibody (M2, Sigma). (D) Arf-like 3 shows specific binding to phosphatidic acid in a GTP binding dependent manner. PIP-strip analysis results of GTP loaded Arl3 (GTP) and GDP loaded Arl3 (GDP) are shown. Spotted lipid species are indicated in the left side (PI3P: PtdIns(3)P, PI4P: PtdIns(4)P, PI5P: PtdIns(5)P, PE: Phosphatidylethanolamine, PC: Phosphatidylcholine, PIP2: PtdIns(4,5)P2, PIP3: PtdIns(3,4,5)P3, PA: Phosphatidic acid, PS: Phosphatidylserine).

Reference

Begele, A., Tryoen-Toth, P., Barry, J., Bader, M. and Vitale, N. (2009) Arf6 regulates the synthesis of fusogenic lipids for calcium-regulated exocytosis in neuroendocrine cells. J. Biol. Chem., in press.

Behnia, R., Panic, B., Whyte, J.R. and Munro, S. (2004) Targeting of the Arf-like GTPase Arl3p to the Golgi requires N-terminal acetylation and the membrane protein Sys1p. Nat Cell Biol 6, 405-13.

Burd, C.G., Strochlic, T.I. and Gangi Setty, S.R. (2004) Arf-like GTPases: not so Arf-like after all. Trends Cell Biol 14, 687-94.

Cavenagh, M., Breiner, M., Schurmann, A., Rosenwald, A., Terui, T., Zhang, C., Randazzo, P, Adams, M., Joost, H. and Kahn, R. (1994) ADP-ribosylation factor (ARF)-like 3, a new member of the ARF family of GTP-binding proteins cloned from human and rat tissues. J. Biol. Chem. 269, 18937-18942.

Chihara, T., Kato, K., Taniguchi, M., Ng, J. and Hayashi, S. (2003) Rac promotes epithelial cell rearrangement during tracheal tubulogenesis in Drosophila. Development 130, 1419-1428.

Crosby, M.A., Goodman, J.L., Strelets, V.B., Zhang, P. and Gelbart, W.M. (2007) FlyBase: genomes by the dozen. Nucleic Acids Res 35, D486-91.

Drysdale, R.A. and Crosby, M.A. (2005) FlyBase: genes and gene models. Nucleic Acids Res 33, D390-5.

D'Souza-Schorey, C. and Chavrier, P. (2006) ARF proteins: roles in membrane traffic and beyond. Nat Rev Mol Cell Biol 7, 347-58.

Foe, V.E., Odell, G.M. and Edgar, B.A. (1993) Mitosis and Morphogenesis in the *Drosophila* Embryo: Point and Counterpoint. In Bate, M. and Martinez-Arias, A. (eds.), The Development of Drosophila melanogaster, Cold Spring Harbor Laboratory Press, New York, Vol. 1, pp. 149-300.

Grayson, C., Bartolini, F., Chapple, J.P., Willison, K.R., Bhamidipati, A., Lewis, S.A., Luthert, P.J., Hardcastle, A.J., Cowan, N.J. and Cheetham, M.E. (2002) Localization in the human retina of the X-linked retinitis pigmentosa protein RP2, its homologue cofactor C and the RP2 interacting protein Arl3. Hum Mol Genet 11, 3065-74.

Gromley, A., Yeaman, C., Rosa, J., Redick, S., Chen, C.T., Mirabelle, S., Guha, M., Sillibourne, J. and Doxsey, S.J. (2005) Centriolin anchoring of exocyst and SNARE complexes at the midbody is required for secretory-vesicle-mediated abscission. Cell 123, 75-87.

Hofmann, I. and Munro, S. (2006) An N-terminally acetylated Arf-like GTPase is localised to lysosomes and affects their motility. J Cell Sci 119, 1494-503.

Hsu, S.C., TerBush, D., Abraham, M. and Guo, W. (2004) The exocyst complex in polarized exocytosis. Int Rev Cytol 233, 243-65.

Ikeya, T. and Hayashi, S. (1999) Interplay of Notch and FGF signaling restricts cell fate

and MAPK activation in the Drosophila trachea. Development 126, 4455-4463.

James, D., Khodthong, C., Kowalchyk, J. and Martin, T. (2008) Phosphatidylinositol 4,5-bisphosphate regulates SNARE-dependent membrane fusion. J. Chem. Biol. 182, 355-366.

Jiang, L., Rogers, S.L. and Crews, S.T. (2007) The Drosophila Dead end Arf-like3 GTPase controls vesicle trafficking during tracheal fusion cell morphogenesis. Developmental Biology in press.

Kahn, R.A., Volpicelli-Daley, L., Bowzard, B., Shrivastava-Ranjan, P., Li, Y., Zhou, C. and Cunningham, L. (2005) Arf family GTPases: roles in membrane traffic and microtubule dynamics. Biochem Soc Trans 33, 1269-72.

Kamei, M., Saunders, W.B., Bayless, K.J., Dye, L., Davis, G.E. and Weinstein, B.M. (2006) Endothelial tubes assemble from intracellular vacuoles in vivo. Nature 442, 453-6.

Katoh, K., Kuma, K., Toh, H. and Miyata, T. (2005) MAFFT version 5: improvement in accuracy of multiple sequence alignment. Nucleic Acids Res 33, 511-8.

Kawasaki, M., Nakayama, K. and Wakatsuki, S. (2005) Membrane recruitment of effector proteins by Arf and Rab GTPases. Curr Opin Struct Biol 15, 681-9.

Kim, S., Shilagardi, K., Zhang, S., Hong, S.N., Sens, K.L., Bo, J., Gonzalez, G.A. and Chen, E.H. (2007) A critical function for the actin cytoskeleton in targeted exocytosis of prefusion vesicles during myoblast fusion. Dev Cell 12, 571-86.

Langevin, J., Morgan, M.J., Sibarita, J.B., Aresta, S., Murthy, M., Schwarz, T., Camonis, J. and Bellaiche, Y. (2005) Drosophila exocyst components Sec5, Sec6, and Sec15 regulate DE-Cadherin trafficking from recycling endosomes to the plasma membrane. Dev Cell 9, 355-76.

Lee, M., Orci, L., Hamamoto, S., Futai, E., Ravazzola, M. and Schekman, R. (2005) Sar1p N-terminal helix initiates membrane curvature and completes the fission of a COPII vesicle. Cell 122, 605-617.

Lee, S. and Kolodziej, P.A. (2002) The plakin Short Stop and the RhoA GTPase are required for E-cadherin-dependent apical surface remodeling during tracheal tube fusion. Development 129, 1509-20.

Lipschutz, J.H. and Mostov, K.E. (2002) Exocytosis: the many masters of the exocyst. Curr Biol 12, R212-4.

Lundmark, R., Doherty, G.J., Vallis, Y., Peter, B.J. and McMahon H.T. (2008) Arf family GTP loading is activated by, and generates, positive membrane curvature. Biochem J 414, 189-94.

Luschnig, S., Batz, T., Armbruster, K. and Krasnow, M.A. (2006) serpentine and vermiform encode matrix proteins with chitin binding and deacetylation domains that limit tracheal tube length in Drosophila. Curr Biol 16, 186-94.

Martens, S. and McMahon, H. (2008) Mechanisms of membrane fusion: disparate players and common principles. Nat. Rev. Mol. Cell Biol. 9, 543-556.

Massarwa, R., Carmon, S., Shilo, B.Z. and Schejter, E.D. (2007) WIP/WASp-based actin-polymerization machinery is essential for myoblast fusion in Drosophila. Dev Cell 12, 557-69.

Murthy, M., Garza, D., Scheller, R.H. and Schwarz, T.L. (2003) Mutations in the exocyst component Sec5 disrupt neuronal membrane traffic, but neurotransmitter release persists. Neuron 37, 433-47.

Nie, Z., Hirsch, D.S. and Randazzo, P.A. (2003) Arf and its many interactors. Curr Opin Cell Biol 15, 396-404.

Page, R.D.M. (1996) TREEVIEW: An application to display phylogenetic trees on personal computers. Computer Applications in the Biosciences 12, 357-358.

Radcliffe, P.A., Vardy, L. and Toda, T. (2000) A conserved small GTP-binding protein Alp41 is essential for the cofactor-dependent biogenesis of microtubules in fission yeast. FEBS Lett 468, 84-8.

Samakovlis, C., Hacohen, N., Manning, G., Sutherland, D.C., Guillemin, K. and Krasnow, M.A. (1996a) Development of the Drosophila tracheal system occurs by a series of morphologically distinct but genetically coupled branching events. Development 122, 1395-407.

Samakovlis, C., Manning, G., Steneberg, P., Hacohen, N., Cantera, R. and Krasnow, M.A. (1996b) Genetic control of epithelial tube fusion during Drosophila tracheal development. Development 122, 3531-3536.

Schrick, J.J., Vogel, P., Abuin, A., Hampton, B. and Rice, D.S. (2006) ADP-ribosylation factor-like 3 is involved in kidney and photoreceptor development. Am J Pathol 168, 1288-98.

Setty, S.R., Strochlic, T.I., Tong, A.H., Boone, C. and Burd, C.G. (2004) Golgi targeting of ARF-like GTPase Arl3p requires its Nalpha-acetylation and the integral membrane protein Sys1p. Nat Cell Biol 6, 414-9.

Shiga, Y., Tanaka-Matakatsu, M. and Hayashi, S. (1996) A nuclear GFP/ beta-galactosidase fusion protein as a marker for morphogenesis in living Drosophila. Dev., Growth Diffn 38, 99-106.

Strauss, O. (2005) The retinal pigment epithelium in visual function. Physiol Rev 85, 845-81.

Sullivan, W., Ashburner, M. and Hawley, R.S. (2000) Drosophila Protocols. Cold Spring Harbor Laboratory Press, Cold Spring Harbor, NY.

Tanaka-Matakatsu, M., Uemura, T., Oda, H., Takeichi, M. and Hayashi, S. (1996) Cadherin-mediated cell adhesion and cell motility in *Drosophila* trachea regulated by the transcription factor Escargot. Development 122, 3697-3705.

Tomancak, P., Beaton, A., Weiszmann, R., Kwan, E., Shu, S., Lewis, S.E., Richards, S., Ashburner, M., Hartenstein, V., Celniker, S.E. and Rubin, G.M. (2002) Systematic determination of patterns of gene expression during Drosophila embryogenesis. Genome Biol 3, RESEARCH0088.

Whiteley, M., Noguchi, P.D., Sensabaugh, S.M., Odenwald, W.F. and Kassis, J.A. (1992) The *Drosophila* gene *escargot* encodes a zinc finger motif found in *snail*-related genes. Mech. Dev. 36, 117-127.

Zhou, C., Cunningham, L., Marcus, A.I., Li, Y. and Kahn, R.A. (2006) Arl2 and Arl3 regulate different microtubule-dependent processes. Mol Biol Cell 17, 2476-87.

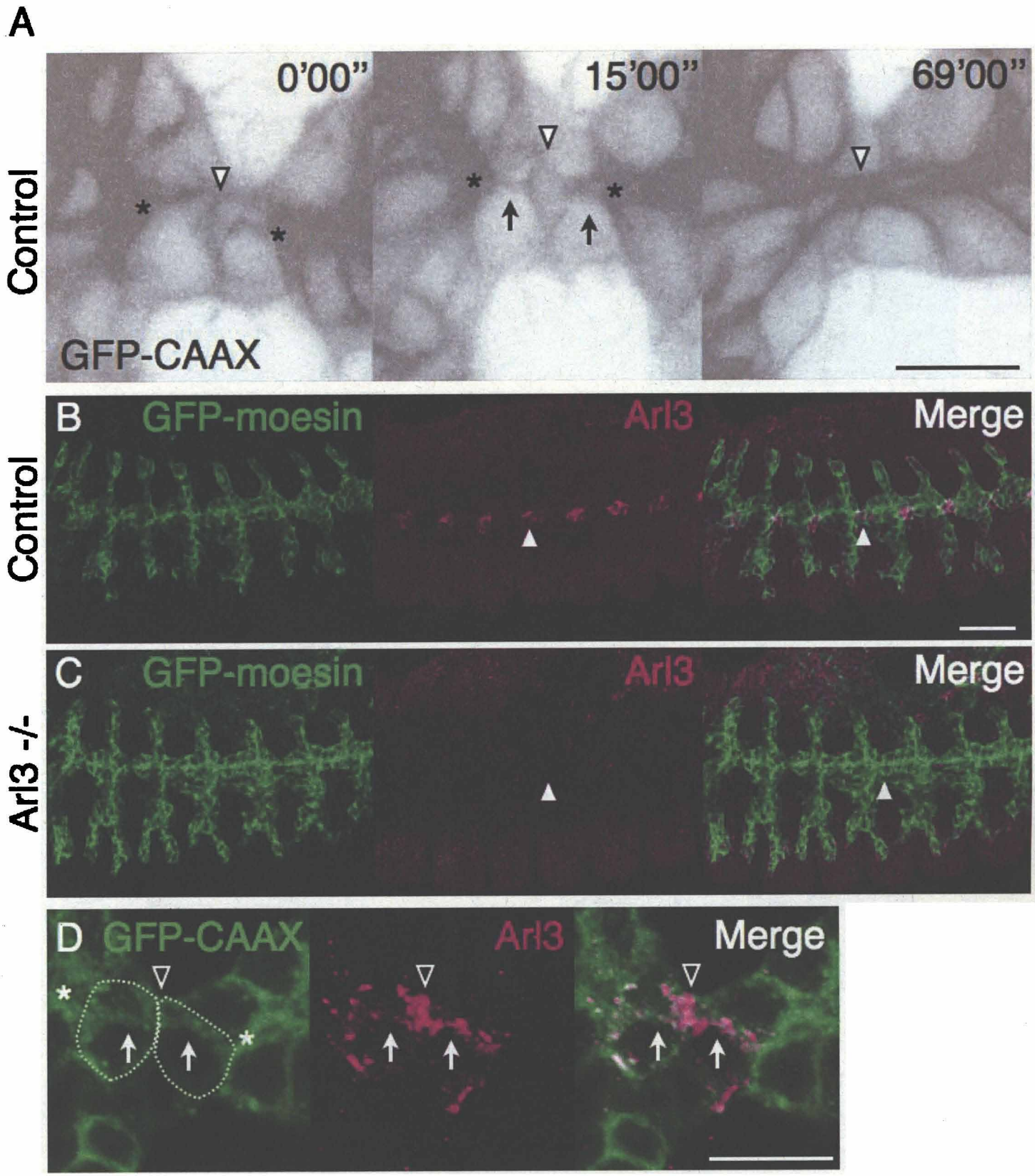
A
Control
0'00"
15'00"
69'00"
GFP-CAAX
B
GFP-moesin
Arl3
Merge
Control
C
GFP-moesin
Arl3
Merge
Arl3 -/-
D
GFP-CAAX
Arl3
Merge

Figure 1

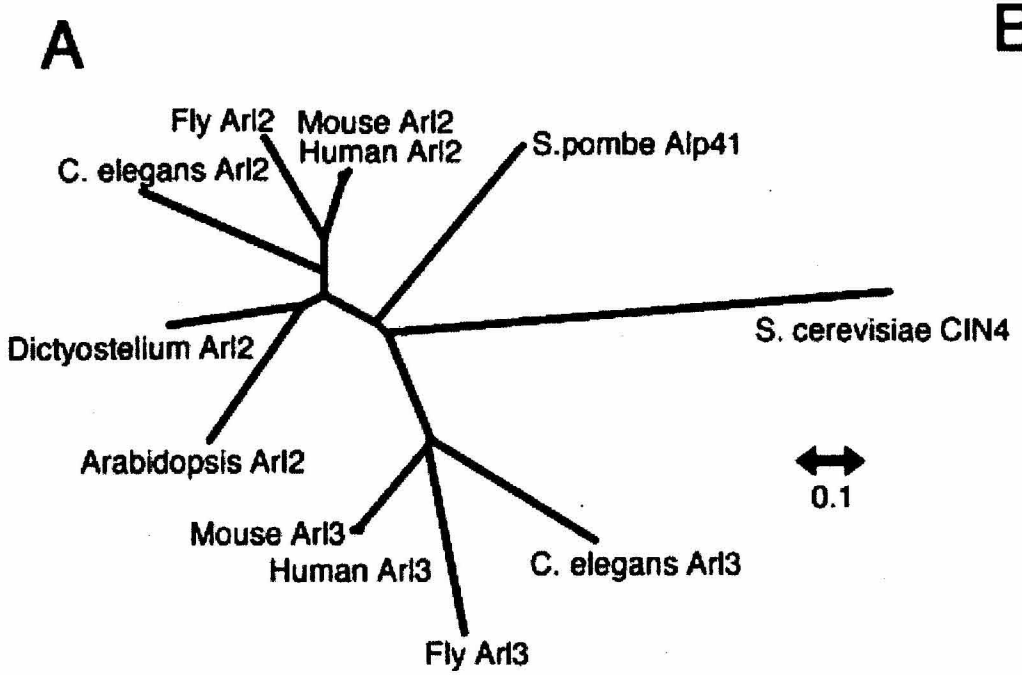
A
Fly Arl2
Mouse Arl2
Human Arl2
C. elegans Arl2
S.pombe Alp41
S. cerevisiae CIN4
Dictyostelium Arl2
Arabidopsis Arl2
Mouse Arl3
Human Arl3
C. elegans Arl3
Fly Arl3
0.1

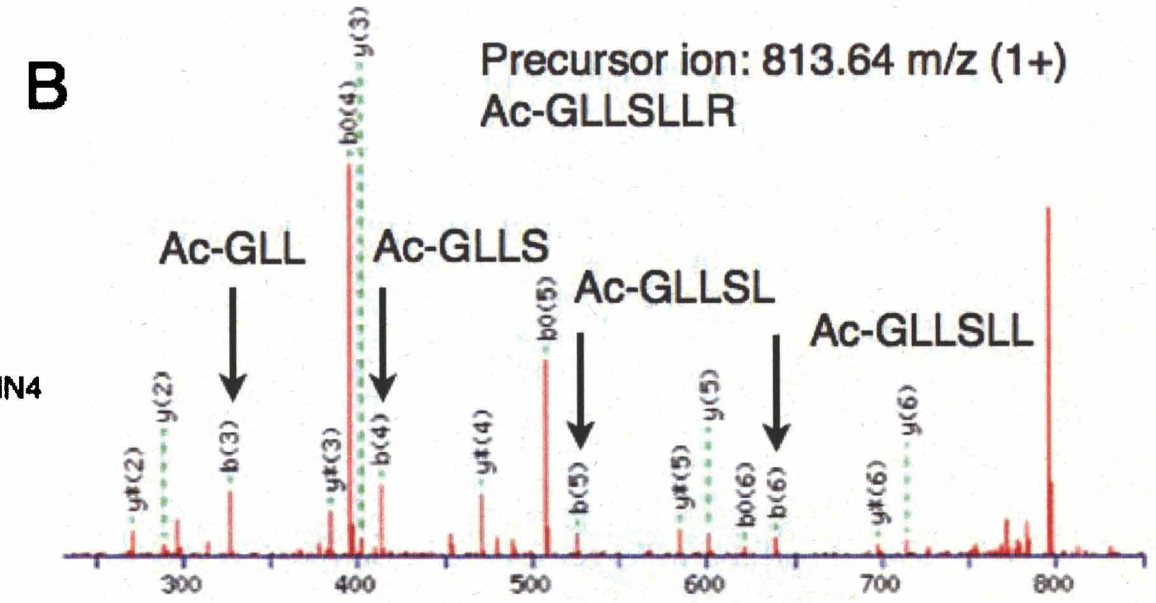
B
Precursor ion: 813.64 m/z (1+)
Ac-GLLSLLR
Ac-GLL
Ac-GLLS
Ac-GLLSL
Ac-GLLSLL
300
400
500
600
700
800

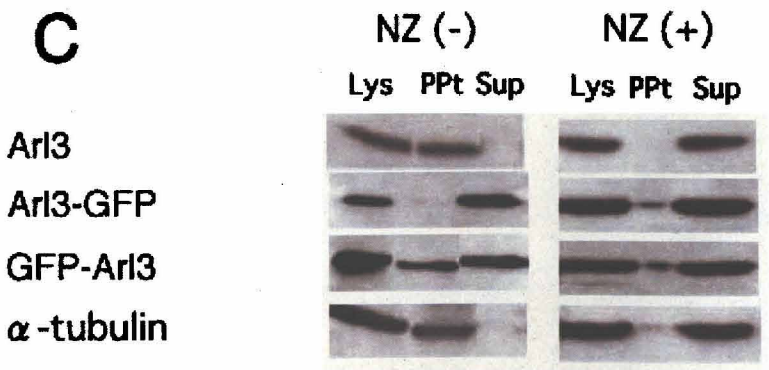
C
NZ (-)
NZ (+)
Lys PPt Sup
Lys PPt Sup
Arl3
Arl3-GFP
GFP-Arl3
α-tubulin

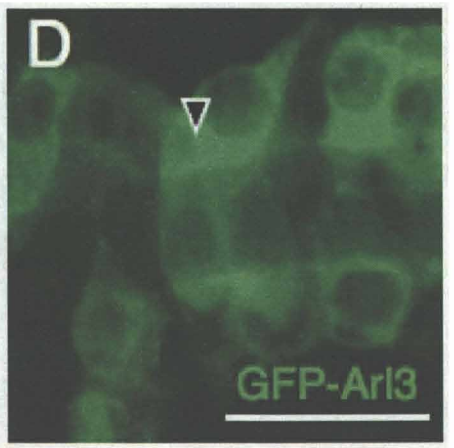
D
GFP-Arl3

Figure 2

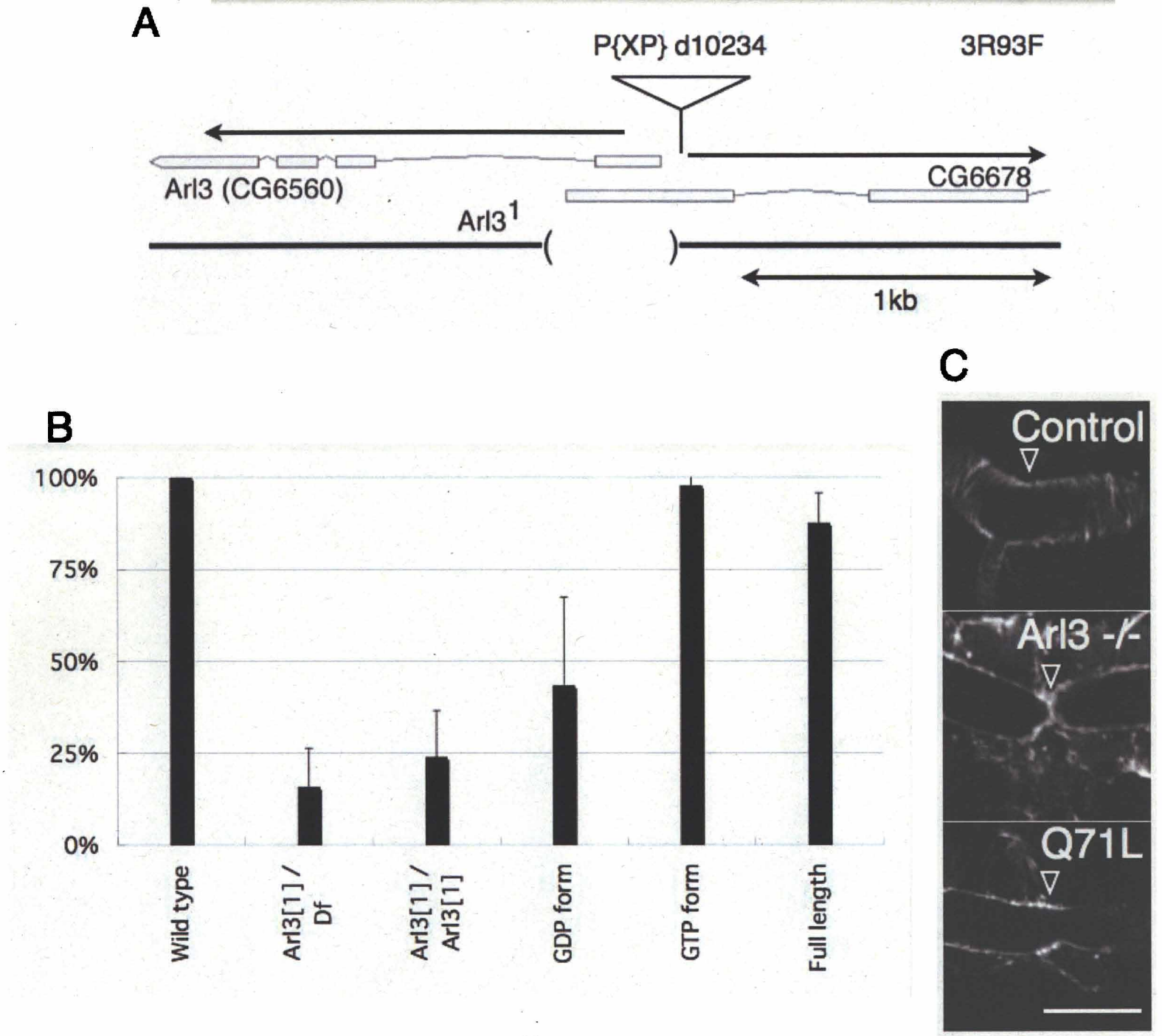
A
P{XP} d10234
3R93F
Arl3 (CG6560)
CG6678
Arl3[1]
1kb
B
100%
75%
50%
25%
0%
Wild type
Arl3[1] / Df
Arl3[1] / Arl3[1]
GDP form
GTP form
Full length
C
Control
Arl3 -/-
Q71L

Figure 3

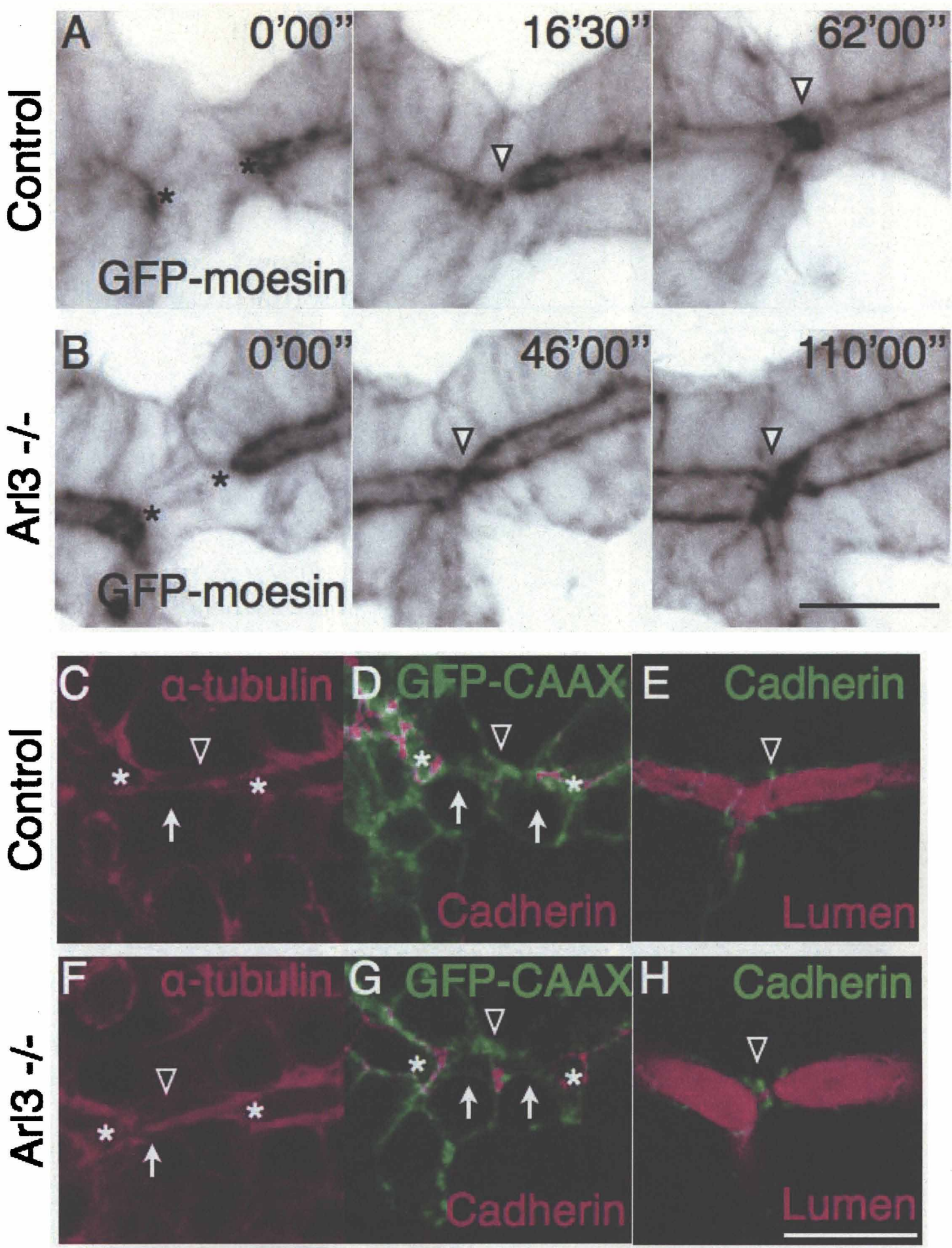
Control
A
0'00"
16'30"
62'00"
GFP-moesin
Arl3 -/-
B
0'00"
46'00"
110'00"
GFP-moesin
Control
C
α-tubulin
D
GFP-CAAX
E
Cadherin
Cadherin
Lumen
Arl3 -/-
F
α-tubulin
G
GFP-CAAX
H
Cadherin
Cadherin
Lumen

Figure 4

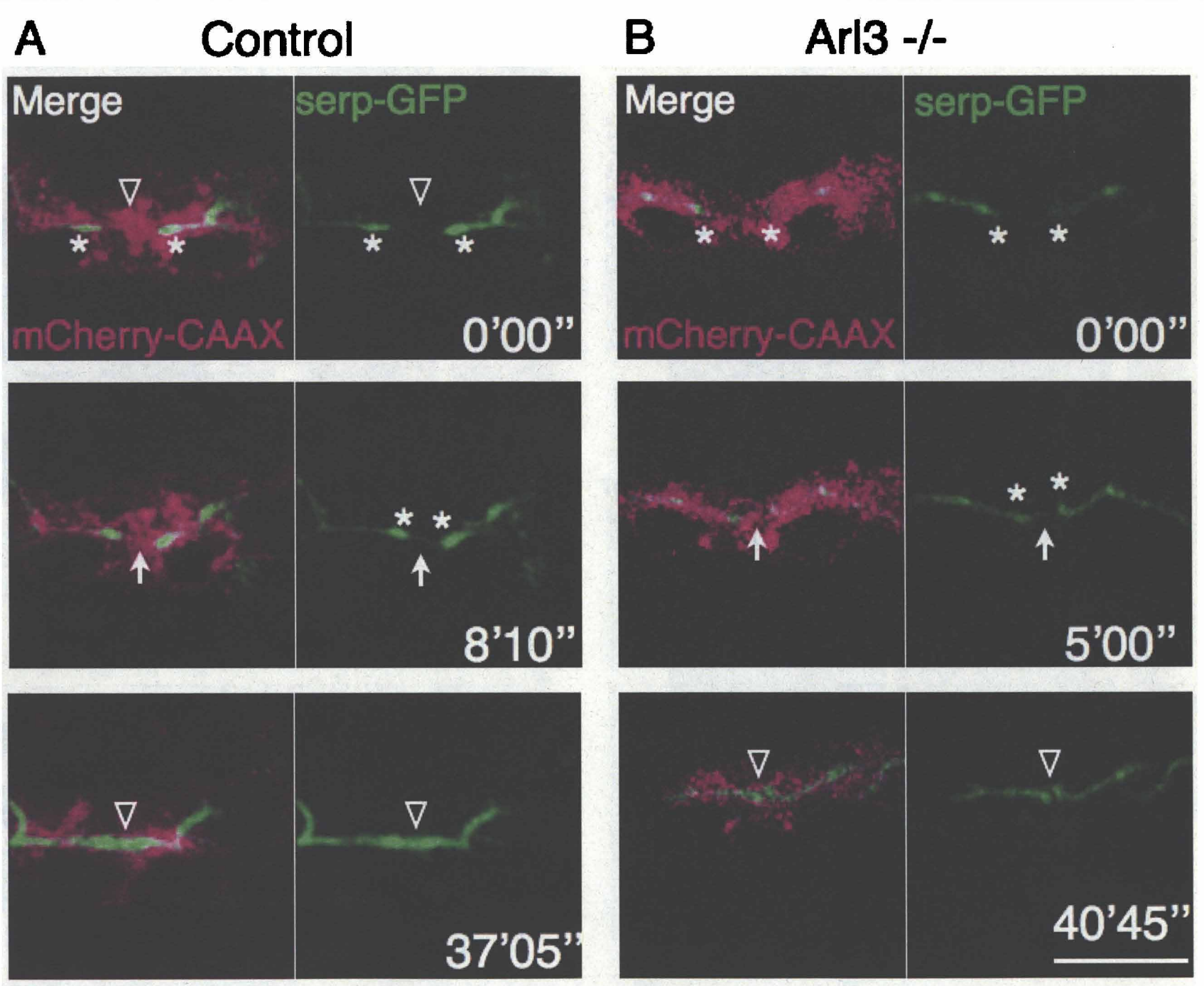
A
Control
B
Arl3 -/-
Merge
serp-GFP
mCherry-CAAX
0'00"
8'10"
5'00"
37'05"
40'45"

Figure 5

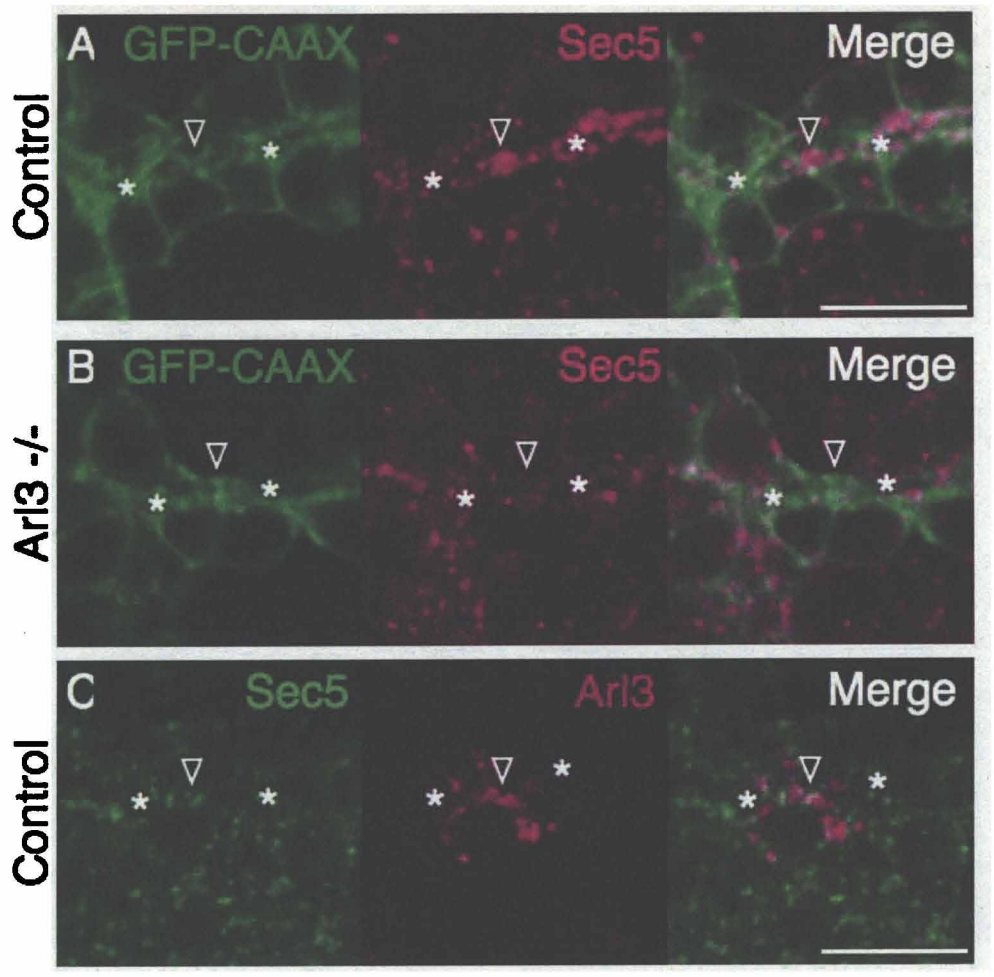
A GFP-CAAX
Sec5
Merge
Control
B GFP-CAAX
Sec5
Merge
Arl3 -/-
C
Sec5
Arl3
Merge
Control

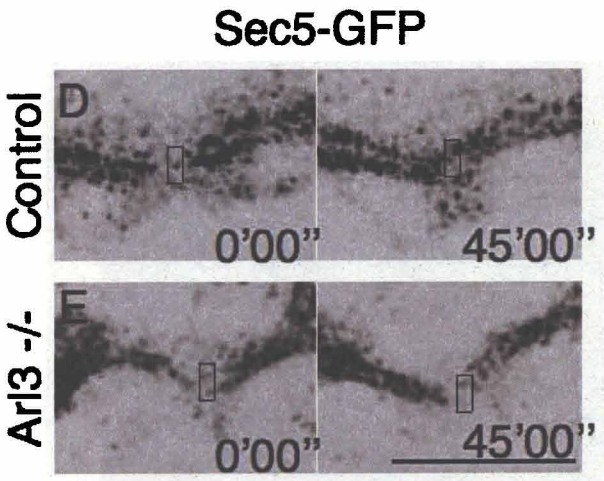
Sec5-GFP
Control
D
0'00"
45'00"
Arl3 -/-
E
0'00"
45'00"

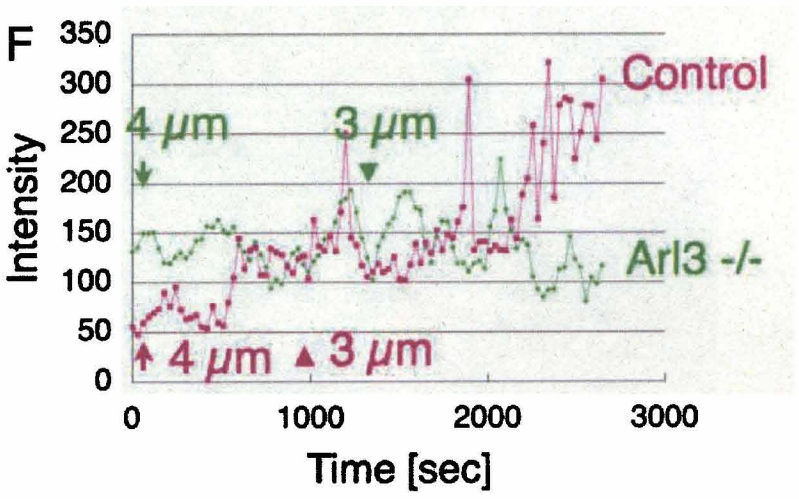
F
Intensity
Time [sec]
Control
Arl3 -/-
4 μm
3 μm
4 μm
3 μm
0
50
100
150
200
250
300
350
0
1000
2000
3000

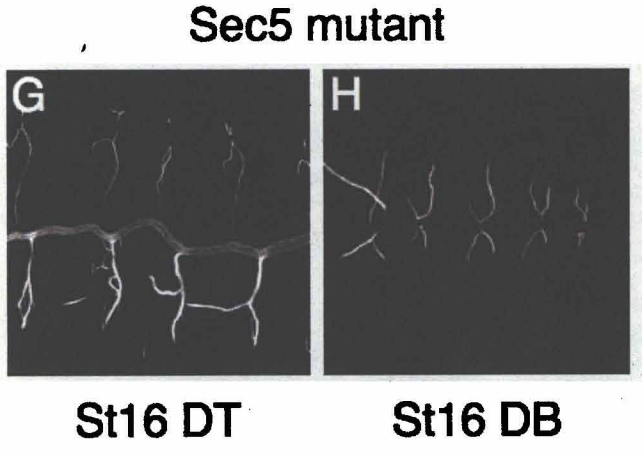
Sec5 mutant
G
H
St16 DT
St16 DB

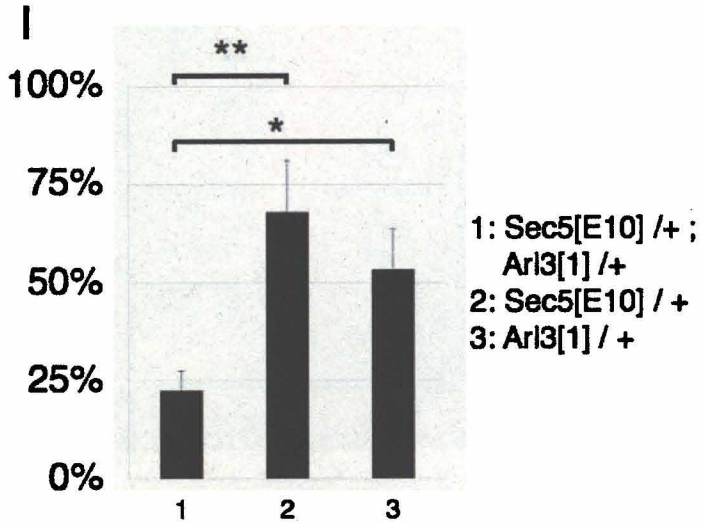
I
**
*
100%
75%
50%
25%
0%
1
2
3
1: Sec5[E10] /+ ;
Arl3[1] /+
2: Sec5[E10] / +
3: Arl3[1] / +

Figure 6

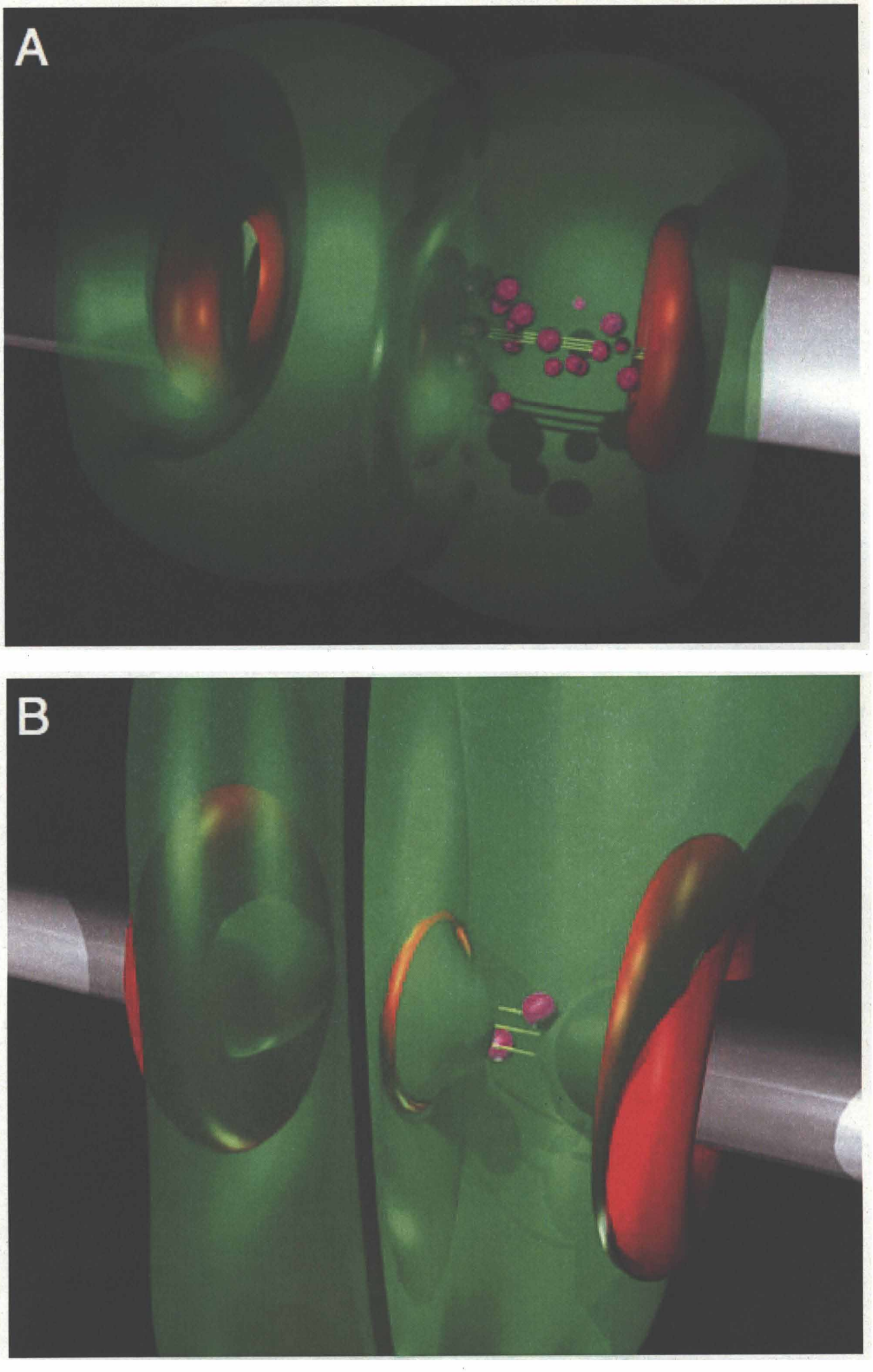

Figure 7

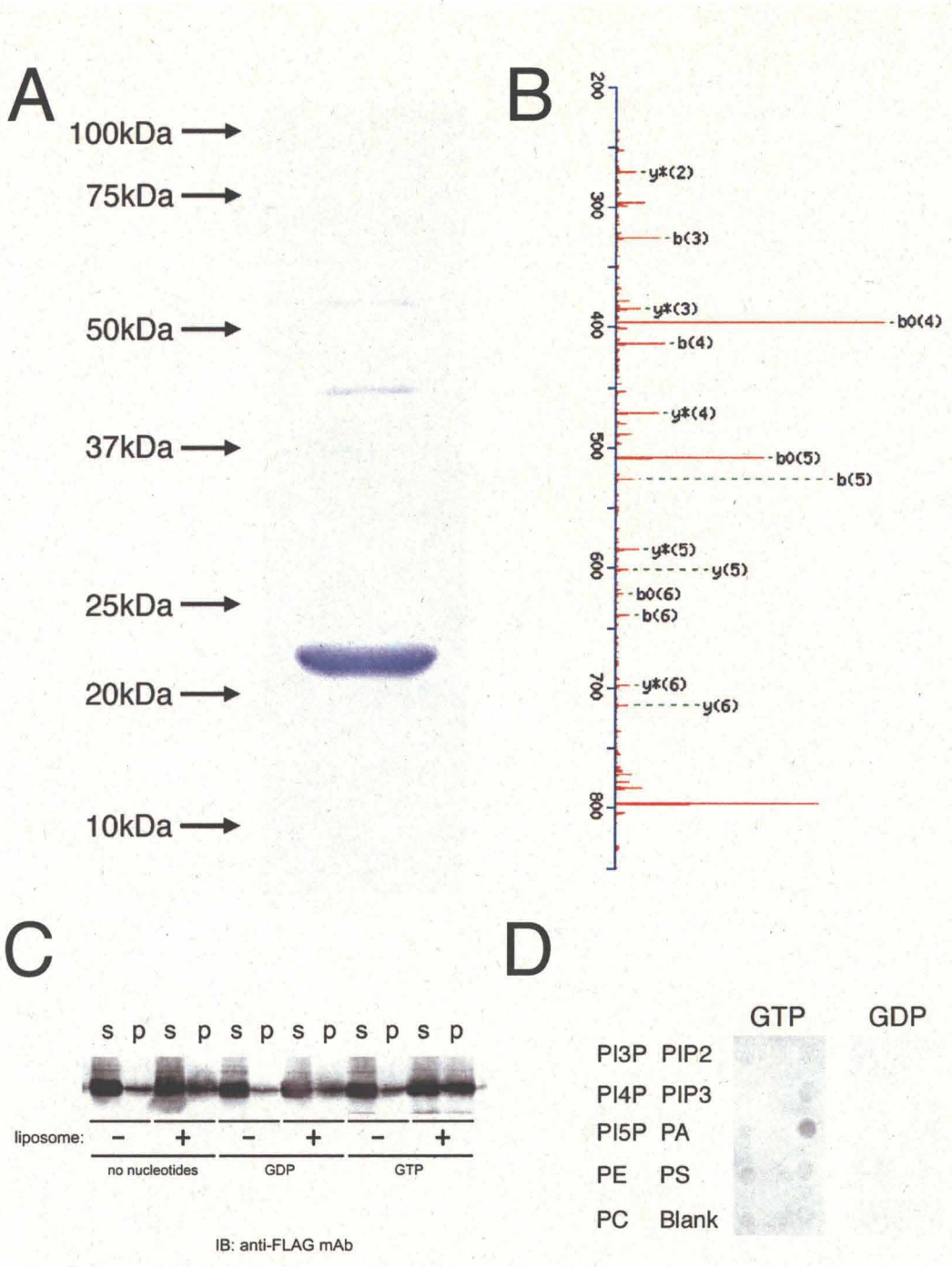
A
100kDa
75kDa
50kDa
37kDa
25kDa
20kDa
10kDa
B
y*(2)
b(3)
y*(3)
b0(4)
b(4)
y*(4)
b0(5)
b(5)
y*(5)
y(5)
b0(6)
b(6)
y*(6)
y(6)
C
s p s p s p s p s p s p
liposome: - + - + - +
no nucleotides
GDP
GTP
IB: anti-FLAG mAb
D
GTP
GDP
PI3P PIP2
PI4P PIP3
PI5P PA
PE PS
PC Blank

Figure 8